

# FACT: FORTRAN toolbox for calculating fluctuations in atomic condensates

Arko Roy<sup>a,b</sup>, Sukla Pal<sup>a,f,\*</sup>, S. Gautam<sup>c</sup>, D. Angom<sup>a</sup>, P. Muruganandam<sup>d,e</sup>

<sup>a</sup>Physical Research Laboratory, Navarangpura, Ahmedabad 380 009, Gujarat, India

<sup>b</sup>Max-Planck-Institut für Physik komplexer Systeme, Nöthnitzer Straße 38, 01187 Dresden, Germany

<sup>c</sup>Department of Physics, Indian Institute of Technology Ropar, Rupnagar, Punjab 14001, India

<sup>d</sup>Department of Physics, Bharathidasan University, Tiruchirappalli 620 024, India

<sup>e</sup>Department of Medical Physics, Bharathidasan University, Tiruchirappalli 620 024, India

<sup>f</sup>Dodd-Walls Centre for Photonic and Quantum Technologies and Department of Physics, University of Otago, Dunedin 9016, New Zealand

---

## Abstract

We develop a FORTRAN code to compute fluctuations in atomic condensates (FACT) by solving the Bogoliubov-de Gennes (BdG) equations for two component Bose-Einstein condensate (TBEC) in quasi-two dimensions. The BdG equations are recast as matrix equations and solved self consistently. The code is suitable for handling quantum fluctuations as well as thermal fluctuations at temperatures below the critical point of Bose-Einstein condensation. The code is versatile, and the ground state density profile and low energy excitation modes obtained from the code can be easily adapted to compute different properties of TBECs — ground state energy, overlap integral, quasi particle amplitudes of BdG spectrum, dispersion relation and structure factor and other related experimental observables.

*Keywords:* Gross-Pitaevskii equation; Hartree-Fock-Bogoliubov theory; Bogoliubov-de Gennes equations; Quasiparticle spectra; Goldstone mode; Kohn/Slosh mode; miscibility-immiscibility transition;

---

## PROGRAM SUMMARY

*Program Title:* FACT

*Journal Reference:*

*Catalogue identifier:*

*Licensing provisions:* none

*Programming language:* FORTRAN 90

*Computer:* Intel Xeon,

*Operating system:* General

*RAM:* at least 1.5Gbytes per core.

*Number of processors used:* 1

---

\*Corresponding author.  
E-mail address: sukla.pal@otago.ac.nz

*Supplementary material:* none

*Classification:*

*External routines/libraries:* ARPACK

*Subprograms used:*

*Journal reference of previous version:\**

*Nature of problem:* Compute the ground state density profile, ground state energy and chemical potential for individual species, evaluate the quasiparticle mode energies and corresponding amplitudes which can capture the transformation of the modes against the change of the parameters (intraspecies interaction, interspecies interaction, anisotropy parameter etc.) using Hartree-Fock Bogoliubov theory with the Popov approximation. Calculate the overlap integral, dispersion relation and structure factor.

*Solution method:* In the first step, the pair of coupled Gross-Pitaevskii equations (CG-PEs) are solved using split time-step Fourier pseudospectral method to compute the condensate density. To solve the BdG equations, as a basic input the first  $N_b$  harmonic oscillator eigenstates are chosen as a basis to generate the BdG matrix with dimension of  $4(N_b + 1) \times 4(N_b + 1)$ . Since the matrix size rapidly increases with  $N_b$ , ARPACK routines are used to diagonalise the BdG matrix efficiently. To compute the fluctuation and non-condensate density, a set of the low energy quasiparticle amplitudes above a threshold value of the Bose factor are considered. The equations are then solved iteratively till the condensate, and non-condensate densities converge to predefined accuracies. To accelerate the convergence we use the method of successive under-relaxation (SUR).

*Restrictions:*

For a large system size, if the harmonic oscillator basis size is also taken to be large, the dimension of the BdG matrix becomes huge. It may take several days to compute the low energy modes at finite temperature and this package may be computationally expensive.

*Additional comments:*

After successful computation of this package, one should obtain the equilibrium density profiles for TBEC, low energy Bogoliubov modes and the corresponding quasiparticle amplitudes. In addition, one can calculate the dispersion relation, structure factor, overlap integral, correlation function, etc. using this package with minimal modifications. In the theory section of the manuscript, we have provided the expressions to compute the above quantities numerically.

*Running time:*

~ 10 minutes for the sample case. For self consistent calculation with 15 iterations, it could take approximately 2 days for the parameters specified in the manuscript.

## 1. Introduction

The self-consistent Hartree-Fock-Bogoliubov theory with the Popov (HFB-Popov) approximation is an effective model to examine the fluctuations of equilibrium state solutions of trapped BEC at zero temperature as well as finite temperatures. The theory is in particular well suited to examine the evolution of the low-lying modes as a function of the interaction parameters, temperature or trapping parameters. It has been used extensively in single-species BEC to study finite temperature effects and mode energies

[1–4], and the results are in good agreement with experimental results [5] at low temperatures. The detailed and systematic information about the quasiparticle spectrum, both of single and multispecies condensate, are described by the HFB formalism. In two-species BECs (TBECs), where the phenomenon of phase-separation is important [6, 7], the HFB-Popov approximation has been used in the miscible [8] and immiscible domain [9–11] to compute the low-lying modes.

In the present work we report the development of a FORTRAN code which implements the HFB-Popov theory to compute the low energy elementary excitations of the TBECs. At  $T = 0$ K, where only the quantum fluctuations are present in the system, the code captures the essence of quantum fluctuations. These are important in the stabilization of quantum droplets in binary BEC mixtures [12–15]. In our recent works [16, 17] we have investigated the elementary excitations in radially symmetric and anisotropic TBECs using the present version of FACt. However, the main strength of HFB-Popov approximation is in encapsulating properties of trapped BEC at finite temperatures, which is more realistic and experimentally relevant. It must be emphasized that our code provides high precision and converged results for  $T \ll T_c$  and computes the low energy excitation modes for TBECs in quasi two dimension. It is worth pointing out here that in 3D the fluctuations are less prominent and mean field theories work very well. That is not the case in 2D. The presence of fluctuations, both thermal and quantum, inhibits real condensation in 2D because of Mermin-Wagner-Hohenberg (MWH) theorem [18, 19]; but undergoes a Berezinskii-Kosterlitz-Thouless (BKT) phase transition [20–23]. With regard to the experimental realization of the box trapping potential [24], our codes are timely and ideal to study 2D multicomponent systems. It must also be mentioned that the HFB-Popov has been used to study quantum and thermal fluctuations in optical lattices [25, 26]. It is to be mentioned here that the HFB-Popov equations belong to the general class of linear response problems and very efficient numerical methods have been developed to solve these equations [27, 28].

An important feature of our implementation, which optimizes the computational requirements, is the absence of any constraints on the symmetry. That is, we implement the code in Cartesian coordinates. The basic and important advantage of this approach is that, our code is very general and applicable to the anisotropic cases where the frequency of the trap in  $x$  and  $y$  directions are different.

## 2. Finite temperature theory for two component BEC

In the dilute limit, when the interparticle interactions are weak, the nonlinear Schrödinger equation (NLSE), also known as the Gross-Pitaevskii equation (GPE) provides a good description of BECs. To incorporate the statics and dynamical properties of TBECs, this equation can be generalized to a pair of CGPEs. This, however, is a description valid at zero temperature  $T = 0$  and they form the basis of our computational scheme. Neglecting the quantum fluctuations, the condensed state of TBEC at  $T = 0$  can be described by the macroscopic wave function  $\phi_1(x, y, t)$  ( $\phi_2(x, y, t)$ ) with energy functional  $E_1[\phi_1]$  ( $E_2[\phi_2]$ ) for the first (second) species. The energy functional of the total

system is

$$\begin{aligned}
E &= E_1 + E_2 + E_{12} \\
&= \iint dx dy \left[ \sum_{i=1}^2 \left( \frac{\hbar^2}{2m_i} |\nabla \phi_i|^2 + V_i(x, y) |\phi_i|^2 + \frac{1}{2} U_{ii} |\phi_i|^4 \right) \right. \\
&\quad \left. + U_{12} |\phi_1|^2 |\phi_2|^2 \right]. \tag{1}
\end{aligned}$$

where  $E_{12}$  is the contribution from the interspecies interaction,  $m_i$  is the mass of the bosonic atom of species  $i$ , and  $V_i(x, y)$  is the external harmonic trapping potential. The interaction strengths are given by  $U_{ij} = 2\pi\hbar^2 a_{ij}/m_{ij}$ , where  $m_{ij}^{-1} = m_i^{-1} + m_j^{-1}$  is the reduced mass for an atom  $i$  and an atom  $j$ . Using these definitions and the mean-field theory, the static and dynamical properties of TBEC, albeit at  $T = 0$ , can be examined through the time-independent CGPE

$$\left[ -\frac{\hbar^2}{2m_i} \nabla^2 + V_i(x, y) + \sum_{j=1}^2 U_{ij} |\phi_j|^2 \right] \phi_i = \mu_i \phi_i, \tag{2}$$

which are obtained by variational minimization of the energy functional  $\mathcal{E} = E - \sum_i \mu_i N_i$  with  $\phi_i^*$  as the parameter of variation. The Eq. (2) forms the starting point of our analysis of TBECs at finite temperatures ( $T \neq 0$ ). At equilibrium, depending upon the relative strengths of intra- ( $U_{ii}$ ) and inter-species ( $U_{12}$ ) interactions, the TBECs may either be in miscible or immiscible phase. The latter is also referred to as phase-separated and we use these two terms interchangeably. The emergence of these phases renders the physics of TBEC drastically different from single-species BEC. And, the natural question is the role of fluctuations, both quantum and thermal, on these phases. For this, the first step is to solve Eqs. (2), and then use the HFB-Popov approximation to calculate the thermal cloud densities.

For  $T \neq 0$ , along with the two coherent condensate clouds, there exist the incoherent non-condensate clouds of both the species. This introduces additional interparticle interactions, the intra- and inter-species interactions between the condensate and non-condensate clouds. The presence of larger number of interaction terms complicates the governing equations, and poses difficulty to theoretically model the system. In the present work, we have assumed that the thermal clouds of both the species are static, and consider  $T$  less than the lower critical temperature among the two.

### 2.1. Hartree Fock Bogoliubov Theory for quasiparticle excitations

To obtain the Hartree Fock Bogoliubov equation we consider the grand-canonical Hamiltonian for TBECs in a quasi-2D trap,

$$\begin{aligned}
\hat{H} &= \sum_{i=1,2} \iint dx dy \hat{\Psi}_i^\dagger(x, y, t) \left[ -\frac{\hbar^2}{2m_i} \left( \frac{\partial^2}{\partial x^2} + \frac{\partial^2}{\partial y^2} \right) + V_i(x, y) - \mu_i \right. \\
&\quad \left. + \frac{U_{ii}}{2} \hat{\Psi}_i^\dagger(x, y, t) \hat{\Psi}_i(x, y, t) \right] \hat{\Psi}_i(x, y, t) \\
&\quad + U_{12} \iint dx dy \hat{\Psi}_1^\dagger(x, y, t) \hat{\Psi}_2^\dagger(x, y, t) \hat{\Psi}_1(x, y, t) \hat{\Psi}_2(x, y, t), \tag{3}
\end{aligned}$$

where  $i = 1, 2$  is the species index,  $\hat{\Psi}_i$ 's are the Bose field operators of the two species, and  $\mu_i$ 's are the chemical potentials. The intra- and interspecies interactions strengths are  $U_{ii} = 2a_{ii}\sqrt{2\pi\lambda}$  and  $U_{12} = 2a_{12}\sqrt{2\pi\lambda}(1 + m_1/m_2)$ , respectively, where  $\lambda = (\omega_z/\omega_\perp)$  is the anisotropy parameter. Here,  $a_{ii}, a_{12}$  represent the  $s$ -wave scattering lengths of intra and inter species interactions respectively. The requirement of having a quasi-2D geometry is satisfied through the following inequalities:  $\lambda \gg 1$ ,  $\hbar\omega_z \gg \mu_i$  [29, 30] and  $\hbar\omega_z \gg k_B T$  (at finite temperature  $T$ ) [10, 31]. Under these constraint conditions, the motion of the trapped atoms will be confined strongly along  $z$  direction and the atoms will remain frozen in the ground state providing a quasi-2D confinement. The Heisenberg equation of motion for the Bose field operators  $\hat{\Psi}_i$  in two-component notation is

$$i\hbar \frac{\partial}{\partial t} \begin{pmatrix} \hat{\Psi}_1 \\ \hat{\Psi}_2 \end{pmatrix} = \begin{pmatrix} \hat{h}_1 + U_{11}\hat{\Psi}_1^\dagger\hat{\Psi}_1 & U_{12}\hat{\Psi}_2^\dagger\hat{\Psi}_1 \\ U_{12}\hat{\Psi}_1^\dagger\hat{\Psi}_2 & \hat{h}_2 + U_{22}\hat{\Psi}_2^\dagger\hat{\Psi}_2 \end{pmatrix} \begin{pmatrix} \hat{\Psi}_1 \\ \hat{\Psi}_2 \end{pmatrix}, \quad (4)$$

where  $\hat{h}_i = (-\hbar^2/2m_i)(\partial^2/\partial x^2 + \partial^2/\partial y^2) + V_i(x, y) - \mu_i$ . Using Bogoliubov approximation, the field operators can be written as  $\hat{\Psi}_i(x, y, t) = \phi_i(x, y) + \tilde{\psi}_i(x, y, t)$ , where  $\phi_i(x, y)$  is a  $c$ -field and represents the condensate, and  $\tilde{\psi}_i(x, y, t)$  is the fluctuation operator corresponding to the  $i$ th species. We can write the total field operator as

$$\begin{pmatrix} \hat{\Psi}_1 \\ \hat{\Psi}_2 \end{pmatrix} = \begin{pmatrix} \phi_1 \\ \phi_2 \end{pmatrix} + \begin{pmatrix} \tilde{\psi}_1 \\ \tilde{\psi}_2 \end{pmatrix}, \Rightarrow \hat{\Psi} = \Phi + \tilde{\Psi}, \quad (5)$$

where  $\Phi$  and  $\tilde{\Psi}$  are the condensate and fluctuation operator in two-component notations. Using the expression of  $\hat{\Psi}_i$ , we can separate the Hamiltonian into terms of different orders in fluctuation operators i.e.  $\hat{H} = \sum_{i=1,2} \sum_{n=0}^4 \hat{H}_n^i$ , where  $0 \leq n \leq 4$  denotes the order of the fluctuation operators. The explicit forms of the fluctuation operators are provided in the Appendix. Following the derivation, the equation of motion of the fluctuation operator for the first species is

$$i\hbar \frac{\partial \tilde{\psi}_1}{\partial t} = \left( -\frac{\hbar^2}{2m_1} \nabla^2 + V_1 + 2U_{11}(n_{1c} + \tilde{n}_1) - \mu_1 + U_{12}|\phi_2|^2 + U_{12}\tilde{n}_2 \right) \tilde{\psi}_1 + U_{11}(\phi_1^2 + \tilde{m}_1) \tilde{\psi}_1^\dagger + U_{12}\phi_1\phi_2^* \tilde{\psi}_2 + U_{12}\phi_1\phi_2 \tilde{\psi}_2^\dagger. \quad (6)$$

where for the same species  $i = j$ , the fluctuation operators are  $\langle \tilde{\psi}_i^\dagger \tilde{\psi}_i \rangle = \tilde{n}_i$ , and  $\langle \tilde{\psi}_i \tilde{\psi}_i \rangle = \tilde{m}_i$ . However, as mentioned  $\langle \tilde{\psi}_i^\dagger \tilde{\psi}_j \rangle = \langle \tilde{\psi}_i \tilde{\psi}_j \rangle = 0$ .

Similarly, the equation of motion of the fluctuation operator of the second species is,

$$i\hbar \frac{\partial \tilde{\psi}_2}{\partial t} = \left( -\frac{\hbar^2}{2m_2} \nabla^2 + V_2 + 2U_{22}(n_{2c} + \tilde{n}_2) - \mu_2 + U_{21}|\phi_1|^2 + U_{21}\tilde{n}_1 \right) \tilde{\psi}_2 + U_{22}(\phi_2^2 + \tilde{m}_2) \tilde{\psi}_2^\dagger + U_{21}\phi_1^* \phi_2 \tilde{\psi}_1 + U_{21}\phi_1\phi_2 \tilde{\psi}_1^\dagger. \quad (7)$$

For compact notation, we have used the definitions  $n_i = n_{ic} + \tilde{n}_i$ , and  $m_i = \phi_i^2 + \tilde{m}_i$ . The next step is to diagonalise the Hamiltonian matrix and obtain the quasiparticle

amplitude functions  $us$  and  $vs$ . Incorporating the Bogoliubov transformation, the fluctuation operators have the following form

$$\tilde{\psi}_i = \sum_j \left[ u_{ij} \hat{\alpha}_j e^{-iE_j t/\hbar} - v_{ij}^* \hat{\alpha}_j^\dagger e^{iE_j t/\hbar} \right], \quad (8a)$$

$$\tilde{\psi}_i^\dagger = \sum_j \left[ u_{ij}^* \hat{\alpha}_j^\dagger e^{iE_j t/\hbar} - v_{ij} \hat{\alpha}_j e^{-iE_j t/\hbar} \right]. \quad (8b)$$

Here,  $j$  is the index representing the sequence of quasiparticle excitations. We take the operators  $\alpha$  and  $\alpha^\dagger$  as common to both the species which is consistent in describing the coupled multispecies dynamics. Furthermore, this reproduces the standard coupled BdG equations at  $T = 0$  and in the limit  $a_{12} \rightarrow 0$ , the quasiparticle spectra separates into two distinct sets: one set for each of the condensates. On substituting Eq. (8) in Eqns. (6) and (7) we obtain the BdG equations for TBEC. And, in scaled units the BdG equations are

$$\hat{\mathcal{L}}_1 u_{1j} - U_{11} \phi_1^2 v_{1j} + U_{12} \phi_1 (\phi_2^* u_{2j} - \phi_2 v_{2j}) = E_j u_{1j}, \quad (9a)$$

$$\hat{\mathcal{L}}_1 v_{1j} + U_{11} \phi_1^{*2} u_{1j} - U_{12} \phi_1^* (\phi_2 v_{2j} - \phi_2^* u_{2j}) = E_j v_{1j}, \quad (9b)$$

$$\hat{\mathcal{L}}_2 u_{2j} - U_{22} \phi_2^2 v_{2j} + U_{12} \phi_2 (\phi_1^* u_{1j} - \phi_1 v_{1j}) = E_j u_{2j}, \quad (9c)$$

$$\hat{\mathcal{L}}_2 v_{2j} + U_{22} \phi_2^{*2} u_{2j} - U_{12} \phi_2^* (\phi_1 v_{1j} - \phi_1^* u_{1j}) = E_j v_{2j}, \quad (9d)$$

where  $\hat{\mathcal{L}}_1 = (\hat{h}_1 + 2U_{11}n_1 + U_{12}n_2)$ ,  $\hat{\mathcal{L}}_2 = (\hat{h}_2 + 2U_{22}n_2 + U_{12}n_1)$ ,  $\hat{\mathcal{L}}_i = -\hat{\mathcal{L}}_i$ , and the quasiparticle amplitudes are normalized as

$$\iint dx dy \sum_i (|u_{ij}(x, y)|^2 - |v_{ij}(x, y)|^2) = 1. \quad (10)$$

Under time-independent HFB-Popov approximation for a TBEC,  $\phi_i$ s are the static solutions of the CGPEs

$$\hat{h}_1 \phi_1 + U_{11} [n_{c1} + 2\tilde{n}_1] \phi_1 + U_{12} n_2 \phi_1 = 0, \quad (11a)$$

$$\hat{h}_2 \phi_2 + U_{22} [n_{c2} + 2\tilde{n}_2] \phi_2 + U_{12} n_1 \phi_2 = 0. \quad (11b)$$

To solve Eq. (9) we define  $u_{ij}$  and  $v_{ij}$ 's as linear combination of  $N_b$  harmonic oscillator eigenstates,

$$\begin{aligned} u_{1j}(x, y) &= \sum_{\kappa, l=0}^{N_b} p_{j\kappa l} \varphi_{\kappa j}(x) \varphi_{l j}(y), & v_{1j}(x, y) &= \sum_{\kappa, l=0}^{N_b} q_{j\kappa l} \varphi_{\kappa j}(x) \varphi_{l j}(y), \\ u_{2j}(x, y) &= \sum_{\kappa, l=0}^{N_b} r_{j\kappa l} \varphi_{\kappa j}(x) \varphi_{l j}(y), & v_{2j}(x, y) &= \sum_{\kappa, l=0}^{N_b} s_{j\kappa l} \varphi_{\kappa j}(x) \varphi_{l j}(y), \end{aligned} \quad (12)$$

where  $\varphi_{k j}$ s and  $\varphi_{l j}$ s are the  $j$ th harmonic oscillator eigenstates and  $p_{j\kappa l}$ ,  $q_{j\kappa l}$ ,  $r_{j\kappa l}$  and  $s_{j\kappa l}$  are the coefficients of linear combination. Using this expansion Eq. (9) is reduced to a matrix eigenvalue equation and solved using standard matrix diagonalization algorithms. The matrix has a dimension of  $4(N_b + 1) \times 4(N_b + 1)$  and is

non-Hermitian, non-symmetric and may have complex eigenvalues. Considering the orthogonality of harmonic oscillator basis, the matrix becomes sparse. Due to the  $N_b^2$  scaling of the BdG matrix, the matrix size rapidly increases with the basis size, and it is essential to use algorithms capable of large matrix diagonalization. For this reason, we use ARPACK [32]. The eigenvalue spectrum obtained from the diagonalization of the matrix has an equal number of positive and negative eigenvalues  $E_j$ 's. Using the quasiparticle amplitudes obtained, the number density  $\tilde{n}_i$  of the non-condensate atoms is

$$\tilde{n}_i = \sum_j \{ [|u_{ij}|^2 + |v_{ij}|^2] N_0(E_j) + |v_{ij}|^2 \}, \quad (13)$$

where  $\langle \hat{\alpha}_j^\dagger \hat{\alpha}_j \rangle = (e^{\beta E_j} - 1)^{-1} \equiv N_0(E_j)$  is the Bose factor of the quasiparticle state with real and positive energy  $E_j$ . The coupled Eqns. (9) and (11) are solved iteratively till the solutions converge to desired accuracy. We use this theory to investigate the evolution of Goldstone modes and mode energies as a function of the interaction strengths and temperature. Although, HFB-Popov does have the advantage vis-a-vis calculation of the modes, it is nontrivial to get converged solutions.

## 2.2. Overlap integral and dispersion relation

A measure of phase separation is the overlap integral,

$$\Lambda = \frac{[\iint n_1(x, y) n_2(x, y) dx dy]^2}{[\iint n_1^2(x, y) dx dy][\iint n_2^2(x, y) dx dy]}. \quad (14)$$

The TBEC is in the miscible phase when  $\Lambda \approx 1$  and signifies complete overlap between the two species when  $\Lambda$  has unit value. The TBEC is completely phase separated when  $\Lambda = 0$  [33]. The other important measure is the response of the TBEC when subjected to external perturbations, and one which defines this is the dispersion relation. To determine the dispersion relation we compute the root mean square of the wave number  $k_j^{\text{rms}}$  of each quasiparticle mode [34, 35]

$$k_j^{\text{rms}} = \left\{ \frac{\sum_i \int d\mathbf{k} k^2 [|u_{ij}(\mathbf{k})|^2 + |v_{ij}(\mathbf{k})|^2]}{\sum_i \int d\mathbf{k} [|u_{ij}(\mathbf{k})|^2 + |v_{ij}(\mathbf{k})|^2]} \right\}^{1/2}. \quad (15)$$

It is to be noted here that  $k_j^{\text{rms}}$  are defined in terms of the quasiparticle modes corresponding to each of the constituent species defined in the  $k$  or momentum space through the index  $i = 1, 2$ . It is then essential to compute  $u_{ij}(\mathbf{k})$  and  $v_{ij}(\mathbf{k})$ , the Fourier transform of the Bogoliubov quasiparticle amplitudes  $u_{ij}(x, y)$  and  $v_{ij}(x, y)$ , respectively. Once we have  $k_j^{\text{rms}}$  for all the modes we obtain a discrete dispersion curve. It is to be mentioned that to obtain  $k_j^{\text{rms}}$ , we consider 2D Fourier transform with  $\mathbf{k} = (k_x, k_y)$  and the integration in Eq. 15 is carried over in 2D Fourier space.

## 2.3. Dynamical structure factor and Correlation function

The dynamical correlation function or the dynamic structure factor (DSF) characterizes the dynamic properties of a quantum many body system and it is a quantity of considerable experimental interest. Unlike other quantum systems where DSF provides

informations ranging from low (characterized by spectrum of collective excitations) to high momentum transfer (characterized by momentum distribution), for BECs of dilute Bose gases DSF is of importance in exploring the domain of high momenta, where the response of the system is not affected by its collective features [36]. Rather it is determined by the momentum distribution of condensate atoms. In experiments DSF is measured by the inelastic light scattering [37] and Bragg spectroscopy [38]. Following refs. [36, 39, 40], the dynamic structure factor in terms of  $j$ th quasi particle amplitudes  $u_{ji}(x, y)$  and  $v_{ji}(x, y)$  for a TBEC is

$$S_d(q_x, q_y, E) = \sum_{j,i} \left| \iint dx dy [u_{ji}^*(x, y) + v_{ji}^*(x, y)] e^{i(xq_x + yq_y)/\hbar} \psi_i(x, y) \right|^2 \delta(E - \epsilon_j), \quad (16)$$

where  $i$  corresponds to the species index and for TBEC system  $i = 1, 2$ .  $\phi_i(x, y)$  is the condensate order parameter for  $i$ th species.

Another important measure of the TBEC which is related to the coherence of the system is the first-order or the off-diagonal correlation function

$$g_i^{(1)}(x, y, x', y') = \frac{\langle \hat{\Psi}_i^\dagger(x, y) \hat{\Psi}_i(x', y') \rangle}{\langle \hat{\Psi}_i^\dagger(x, y) \hat{\Psi}_i(x, y) \rangle \langle \hat{\Psi}_i^\dagger(x', y') \hat{\Psi}_i(x', y') \rangle}, \quad (17)$$

which is also measure of the phase fluctuations. It can also be expressed in terms of off-diagonal condensate and noncondensate densities as

$$g_i^{(1)}(x, y, x', y') = \frac{n_{ci}(x, y; x', y') + \tilde{n}_i(x, y; x', y')}{\sqrt{n_i(x, y) n_i(x', y')}}, \quad (18)$$

where

$$n_{ci}(x, y; x', y') = \phi_i^*(x, y) \phi_i(x', y'), \quad (19)$$

$$\begin{aligned} \tilde{n}_i(x, y; x', y') &= \sum_j \{ [u_{ij}^*(x, y) u_{ij}(x', y') + v_{ij}^*(x, y) v_{ij}(x', y')] N_0(E_j) \\ &+ v_{ij}^*(x, y) v_{ij}(x', y') \} \end{aligned} \quad (20)$$

At  $T = 0$ , when the entire system is coherent and characterized by the presence of a condensate only, then  $g_i^{(1)} = 1$  within the extent of the condensate, whether it is in the miscible or in the immiscible regime. So, one cannot distinguish between the two phases from the nature of the correlation functions of the individual species. However, at  $T \neq 0$ , a clear signature of a miscible-immiscible transition of the density profiles is reflected in the form of correlation functions.

### 3. Details of implementation

#### 3.1. GPE solver and details of basis

As a first step to compute the BdG matrix and derive the BdG equations, we solve the pair of CGP Eqs. (11) using split time-step Crank-Nicolson [41–44] and Fourier-pseudospectral method adapted for binary condensates. The method when implemented with imaginary time propagation is appropriate to obtain the stationary ground

state wave function of the TBEC. However, this is not the only method to solve CGP Eqs. Thorough reviews of various numerical methods to solve GP equation, including the one we have used, are given in refs. [45, 46]. The other numerical methods given in these reviews can as well be adapted to obtain the ground state wave function of TBEC. It must also be added that a description of selected numerical methods to solve multicomponent BECs is reviewed in ref. [47]. To represent the quasiparticle amplitudes  $us$  and  $vs$  as a linear combination of  $N_b$  direct product states  $\varphi(x) \otimes \varphi(y)$  as defined in Eq. (12),  $\varphi(x)$  and  $\varphi(y)$  are considered to be the harmonic oscillator eigenstates [48, 49]. To generate  $\varphi(x)$  and  $\varphi(y)$ , we start with the ground  $\varphi_0(x)$  and first excited state  $\varphi_1(x)$ , and higher excited states are generated using the following recurrence relations

$$H_{n+1}(x) = 2xH_n(x) - 2nH_{n-1}(x) \quad (21)$$

$$\varphi_n(x) = \sqrt{2/n}x\varphi_{n-1}(x) - \sqrt{\frac{n-1}{n}}\varphi_{n-2}(x) \quad (22)$$

where  $H_n(x)$  is the  $n$ th order Hermite polynomial. With this choice both the CGP and BdG equations are solved using pseudospectral methods. The computation of basis function is implemented in the subroutine `basis.f90` and stored on a grid.

### 3.2. BdG matrix in terms of coefficients

The BdG matrix from the set of BdG Eqs.(9) can be written as

$$E \begin{pmatrix} pq \\ rs \end{pmatrix} = \begin{pmatrix} \text{BdG}_{00} & \text{BdG}_{10} \\ \text{BdG}_{01} & \text{BdG}_{11} \end{pmatrix} \begin{pmatrix} pq \\ rs \end{pmatrix}, \quad (23)$$

where the submatrices in the above matrix equation are defined as

$$\text{BdG}_{00} = \begin{pmatrix} \mathcal{A}_{00} & \cdots & \mathcal{A}_{0N_b} & \mathcal{B}_{00} & \cdots & \mathcal{B}_{0N_b} \\ \vdots & \ddots & \vdots & \vdots & \ddots & \vdots \\ \mathcal{A}_{N_b 0} & \cdots & \mathcal{A}_{N_b N_b} & \mathcal{B}_{N_b 0} & \cdots & \mathcal{B}_{N_b N_b} \\ \mathcal{E}_{00} & \cdots & \mathcal{E}_{0N_b} & \mathcal{F}_{00} & \cdots & \mathcal{F}_{0N_b} \\ \vdots & \ddots & \vdots & \vdots & \ddots & \vdots \\ \mathcal{E}_{N_b 0} & \cdots & \mathcal{E}_{N_b N_b} & \mathcal{F}_{N_b 0} & \cdots & \mathcal{F}_{N_b N_b} \end{pmatrix}, \quad (24)$$

$$\text{BdG}_{10} = \begin{pmatrix} \mathcal{C}_{00} & \cdots & \mathcal{C}_{0N_b} & \mathcal{D}_{00} & \cdots & \mathcal{D}_{0N_b} \\ \vdots & \ddots & \vdots & \vdots & \ddots & \vdots \\ \mathcal{C}_{N_b 0} & \cdots & \mathcal{C}_{N_b N_b} & \mathcal{D}_{N_b 0} & \cdots & \mathcal{D}_{N_b N_b} \\ \mathcal{G}_{00} & \cdots & \mathcal{G}_{0N_b} & \mathcal{H}_{00} & \cdots & \mathcal{H}_{0N_b} \\ \vdots & \ddots & \vdots & \vdots & \ddots & \vdots \\ \mathcal{G}_{N_b 0} & \cdots & \mathcal{G}_{N_b N_b} & \mathcal{H}_{N_b 0} & \cdots & \mathcal{H}_{N_b N_b} \end{pmatrix}, \quad (25)$$

$$\text{BdG}_{01} = \begin{pmatrix} \mathcal{I}_{00} & \cdots & \mathcal{I}_{0N_b} & \mathcal{J}_{00} & \cdots & \mathcal{J}_{0N_b} \\ \vdots & \ddots & \vdots & \vdots & \ddots & \vdots \\ \mathcal{I}_{N_b 0} & \cdots & \mathcal{I}_{N_b N_b} & \mathcal{J}_{N_b 0} & \cdots & \mathcal{J}_{N_b N_b} \\ \mathcal{M}_{00} & \cdots & \mathcal{M}_{0N_b} & \mathcal{N}_{00} & \cdots & \mathcal{N}_{0N_b} \\ \vdots & \ddots & \vdots & \vdots & \ddots & \vdots \\ \mathcal{M}_{N_b 0} & \cdots & \mathcal{M}_{N_b N_b} & \mathcal{N}_{N_b 0} & \cdots & \mathcal{N}_{N_b N_b} \end{pmatrix}, \quad (26)$$

$$\text{BdG}_{11} = \begin{pmatrix} \mathcal{K}_{00} & \cdots & \mathcal{K}_{0N_b} & \mathcal{L}_{00} & \cdots & \mathcal{L}_{0N_b} \\ \vdots & \ddots & \vdots & \vdots & \ddots & \vdots \\ \mathcal{K}_{N_b 0} & \cdots & \mathcal{K}_{N_b N_b} & \mathcal{L}_{N_b 0} & \cdots & \mathcal{L}_{N_b N_b} \\ \mathcal{O}_{00} & \cdots & \mathcal{O}_{0N_b} & \mathcal{P}_{00} & \cdots & \mathcal{P}_{0N_b} \\ \vdots & \ddots & \vdots & \vdots & \ddots & \vdots \\ \mathcal{O}_{N_b 0} & \cdots & \mathcal{O}_{N_b N_b} & \mathcal{P}_{N_b 0} & \cdots & \mathcal{P}_{N_b N_b} \end{pmatrix}, \quad (27)$$

$$pq = \begin{pmatrix} p_{00} \\ \vdots \\ p_{N_b N_b} \\ q_{00} \\ \vdots \\ q_{N_b N_b} \end{pmatrix}, \quad (28)$$

$$rs = \begin{pmatrix} r_{00} \\ \vdots \\ r_{N_b N_b} \\ s_{00} \\ \vdots \\ s_{N_b N_b} \end{pmatrix}. \quad (29)$$

The BdG matrix is non-Hermitian and non-symmetric with a dimension of  $4(N_b + 1) \times 4(N_b + 1)$ , so it can have both real and complex eigenvalues depending on the physical parameters of the system under study.

The eigenvalue spectrum obtained from the diagonalization of the matrix has an equal number of positive and negative eigenvalues  $E_j$ 's. From the structure of the matrix elements, we can identify 16 blocks ( $\mathcal{A}, \mathcal{B}, \mathcal{C}, \mathcal{D}, \dots, \mathcal{P}$ ) in the BdG matrix in Eq. (23) and in subroutine `hfb2d2s.f90`, we compute the matrix elements for these blocks. In subroutine `hfb2d2s.f90`, the blocks  $\mathcal{A}, \mathcal{B}, \mathcal{C}, \mathcal{D}, \dots, \mathcal{P}$  correspond to block 1, 2, 3, 4,  $\dots$ , 16. The elements of each block have the following general expressions

$$\begin{aligned}
\mathcal{A}_{pq} &= \iint \varphi_p(x, y) [h_1 + 2U_{11}(n_{1c} + \tilde{n}_1) + U_{12}(n_{2c} + \tilde{n}_2)] \varphi_q(x, y) dx dy, \\
\mathcal{B}_{pq} &= \iint \varphi_p(x, y) [-U_{11}\phi_1^2] \varphi_q(x, y) dx dy, \\
\mathcal{C}_{pq} &= \iint \varphi_p(x, y) [U_{12}\phi_1\phi_2^*] \varphi_q(x, y) dx dy, \\
\mathcal{D}_{pq} &= \iint \varphi_p(x, y) [-U_{12}\phi_1\phi_2] \varphi_q(x, y) dx dy, \\
\mathcal{E}_{pq} &= \iint \varphi_p(x, y) [U_{11}\phi_1^{*2}] \varphi_q(x, y) dx dy, \\
\mathcal{F}_{pq} &= - \iint \varphi_p(x, y) [h_1 + 2U_{11}(n_{1c} + \tilde{n}_1) + U_{12}(n_{2c} + \tilde{n}_2)] \varphi_q(x, y) dx dy, \\
\mathcal{G}_{pq} &= \iint \varphi_p(x, y) [U_{12}\phi_1^*\phi_2^*] \varphi_q(x, y) dx dy, \\
\mathcal{H}_{pq} &= \iint \varphi_p(x, y) [-U_{12}\phi_1^*\phi_2] \varphi_q(x, y) dx dy, \\
\mathcal{I}_{pq} &= - \iint \varphi_p(x, y) [-U_{12}\phi_1^*\phi_2] \varphi_q(x, y) dx dy, \\
\mathcal{J}_{pq} &= \iint \varphi_p(x, y) [-U_{12}\phi_1\phi_2] \varphi_q(x, y) dx dy, \\
\mathcal{K}_{pq} &= \iint \varphi_p(x, y) [h_2 + 2U_{22}(n_{2c} + \tilde{n}_2) + U_{12}(n_{1c} + \tilde{n}_1)] \varphi_q(x, y) dx dy, \\
\mathcal{L}_{pq} &= \iint \varphi_p(x, y) [-U_{22}\phi_2^2] \varphi_q(x, y) dx dy, \\
\mathcal{M}_{pq} &= \iint \varphi_p(x, y) [U_{12}\phi_1^*\phi_2^*] \varphi_q(x, y) dx dy, \\
\mathcal{N}_{pq} &= - \iint \varphi_p(x, y) [U_{12}\phi_1\phi_2^*] \varphi_q(x, y) dx dy, \\
\mathcal{O}_{pq} &= \iint \varphi_p(x, y) [-U_{22}\phi_2^{*2}] \varphi_q(x, y) dx dy, \\
\mathcal{P}_{pq} &= - \iint \varphi_p(x, y) [h_2 + 2U_{22}(n_{2c} + \tilde{n}_2) + U_{12}(n_{1c} + \tilde{n}_1)] \varphi_q(x, y) dx dy.
\end{aligned}$$

The BdG matrix is sparse as the harmonic oscillator basis are orthonormal. So, we use sparse matrix representation to store the matrix, and diagonalized using ARPACK [32] in the subroutine `hfbpopov.f`. Depending on the parameters, from the diagonalization we compute the lowest  $D$  eigenvalues and corresponding  $V$  eigenvectors.

### 3.3. Computations of $u$ and $v$

From the eigenvectors of the BdG matrix, we compute the quasiparticle amplitudes  $u$  and  $v$  in the subroutine `hfb2d2s.f90`. Considering the array of eigenvectors  $V$ ,

from Eq. 12 the quasiparticle amplitudes are computed as

$$u_{1j}(x, y) = \sum_{\kappa, l=0}^{N_b} v_{n_{\kappa l}}^j \varphi_{\kappa}(x) \varphi_l(y); \quad 0 \leq n_{\kappa l} \leq (N_b + 1)^2 - 1, \quad (31)$$

$$v_{1j}(x, y) = \sum_{\kappa, l=0}^{N_b} v_{n_{\kappa l}}^j \varphi_{\kappa}(x) \varphi_l(y); \quad (N_b + 1)^2 \leq n_{\kappa l} \leq 2(N_b + 1)^2 - 1, \quad (32)$$

$$u_{2j}(x, y) = \sum_{\kappa, l=0}^{N_b} v_{n_{\kappa l}}^j \varphi_{\kappa}(x) \varphi_l(y); \quad 2(N_b + 1)^2 \leq n_{\kappa l} \leq 3(N_b + 1)^2 - 1 \quad (33)$$

$$v_{2j}(x, y) = \sum_{\kappa, l=0}^{N_b} v_{n_{\kappa l}}^j \varphi_{\kappa}(x) \varphi_l(y); \quad 3(N_b + 1)^2 \leq n_{\kappa l} \leq 4(N_b + 1)^2 - 1 \quad (34)$$

Here  $j$  is the eigenvalue index,  $v_{n_{\kappa l}}^j$  is the component of the eigenvector and  $n_{\kappa l} \in [0, 4(N_b + 1)^2 - 1]$  is the combined index to identify the components of the eigenvectors *vis-a-vis* the 1D harmonic oscillator basis. The non-degenerate *us* and *vs* are orthonormal. However, to make the degenerate *us* and *vs* orthonormal, we use the Gram–Schmidt orthogonalization scheme.

#### 3.4. Bose factor and Goldstone modes

Once the eigenvalues ( $E_j$ ) of the BdG matrix are obtained after diagonalization, the Bose factor of the  $j$ th state in Eq. (35) is

$$N_0(E_j) = \frac{1}{e^{\beta E_j} - 1}, \quad (35)$$

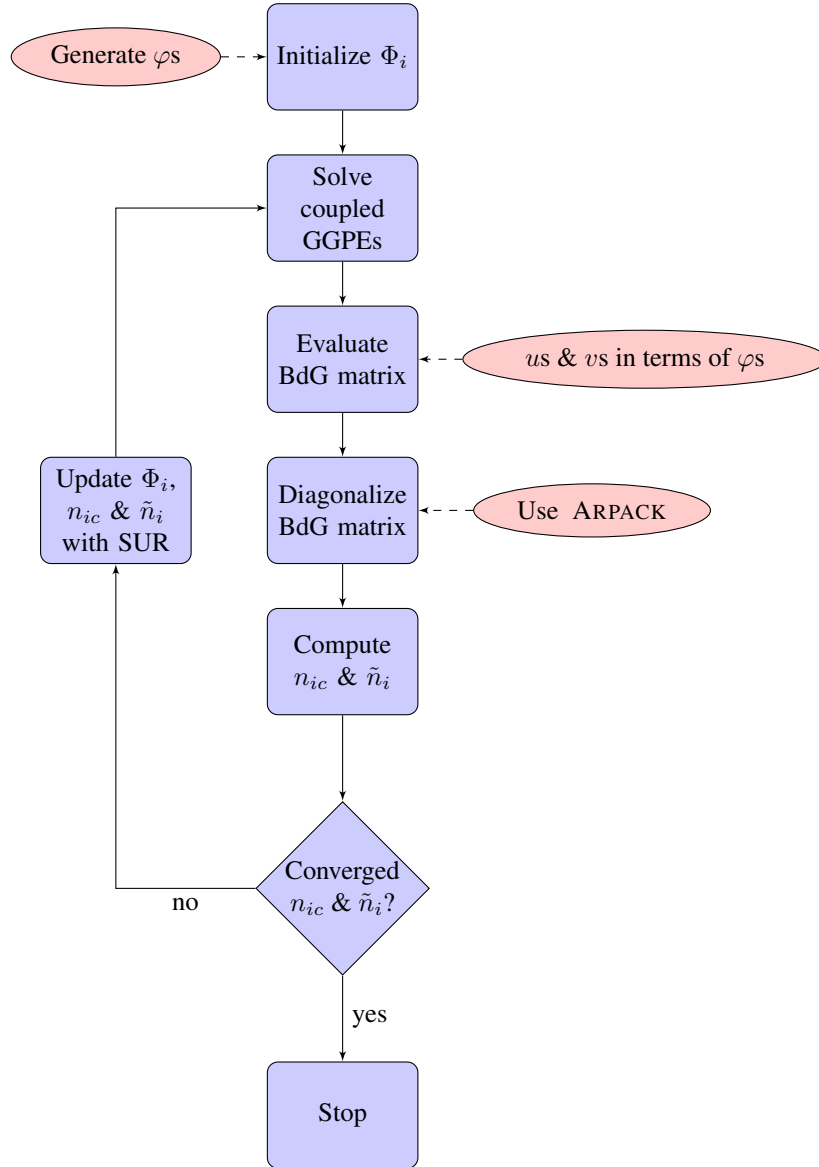
and the corresponding thermal or non-condensate components are computed using the definition of  $\tilde{n}_i$  in Eq.(13). As mentioned earlier, for the degenerate states to render the *us* and *vs* orthonormal we use the Gram-Schmidt orthogonalization. Among the low-energy collective modes, a few are zero energy, and these are the the Nambu-Goldstone (NG) modes. For TBEC, there exists two NG modes for each of the condensate species due to the breaking of  $U(1)$  global gauge symmetry when BEC is formed. These NG modes do not contribute to  $\tilde{n}_i$ , and must be skipped while computing  $\tilde{n}_i$ . This is implemented through the parameter `SKIP = 4` in the main subroutine. In the subroutine `hfb2d2s.f90`, we compute the quasi-particle amplitudes corresponding to these NG modes separately.

The solutions are iterated until  $n_{ic}$  and  $\tilde{n}_i$  converge to a predefined accuracy parameter. For  $T \neq 0$ , the convergence is either very slow due to the thermal fluctuations or tend to diverge. To accelerate the convergence and ameliorate divergence, we use the method of *successive under relaxation* (SUR)[50], and choose the underrelaxation parameter  $S = 0.1$ . The new solution at the  $k$ th iteration is then

$$\phi_k^{\text{new}}(x, y) = S\phi_k(x, y) + (1 - S)\phi_{k-1}(x, y), \quad (36)$$

where  $k$  is the iteration index. To compute  $\tilde{n}_i$  we consider the modes with  $N_0(E_j)$  larger than a threshold value, say  $10^{-3}$ . For parameters relevant to experiments, this is achieved by considering the first 250 or less number of modes.

To show the structure of the code, we show a flowchart which describes the how different modules of the code are related.



#### 4. Description of FACT

##### 4.1. Input file and parameters

This package requires a single input data file `input.dat`. It consists of ten lines, and description of the input parameters are provided in the contents of the sample file

input .dat given below for  $^{133}\text{Cs}$  - $^{87}\text{Rb}$  TBEC in miscible regime shown below.

```

280.0D0   100.0D0   100.0D0   100.0D0   !Scattering lengths  G011,G012,G021,G022
133.0D0           87.0D0           !Masses              M1, M2
8.0D0           !Freq. along X drn.  NUR
1.0D0           12.5D0           !Anisotropy         AL, LAMBDA
2000.0D0        2000.0D0        !Number of atoms    TN01, TN02
0.1D0           !Underrelaxation    SUNDER
55      55      !Basis along X, Y   NBX, NBY
200     250     !NEV NCV
0.0D-9        !Temperature        TEMPK
4          1     !SKIP, ITMAX

```

Where, the parameters are related to various physically significant parameters and these are as follows:

G011, G022:  $s$ -wave scattering lengths of intraspecies interaction for species 1 and species 2 respectively,  
G012, G021:  $s$ -wave scattering lengths of interspecies interaction between species 1 and 2,  
M1, M2 : Mass of species 1 and species 2 respectively,  
NUR : Frequency along  $x$  direction,  
AL : Anisotropy parameter in quasi-2D confinement. ( $AL = \omega_y/\omega_x$ ),  
LAMBDA : Anisotropy parameter to create quasi-2D confinement. ( $LAMBDA = \omega_z/\omega_x$ ),  
TN01, TN02: Total number of atoms of species 1 and 2 respectively,  
SUNDER : Under relaxation parameter to ensure convergence,  
NBX, NBY : Number of harmonic oscillator basis taken into account to construct BdG matrix,  
NEV, NCV : Number of eigenvalues and eigen vectors ARPACK will print in output file,  
TEMPK : Temperature of the system in Kelvin,  
SKIP : Number of Goldstone modes,  
ITMAX : Number of HFB Popov self consistent iteration that will ensure convergence,

where, the scattering lengths are in the units of Bohr radius ( $a_0$ ) and the masses are in the units of amu (atomic mass unit) The above sample input file corresponds to the case of radially symmetric ( $AL = 1$ )  $^{133}\text{Cs}$  - $^{87}\text{Rb}$  TBEC at zero temperature. To examine the effect of anisotropy in the trapping parameters one can consider  $AL < 1$  (corresponding to  $\omega_y \ll \omega_x$ , the TBEC is elongated along  $y$  axis) or  $AL > 1$  (corresponding to  $\omega_x \ll \omega_y$ , the TBEC is elongated along  $x$  axis). In our recent work [17], we have considered the effect of anisotropy in  $^{85}\text{Rb}$  - $^{87}\text{Rb}$  TBEC at zero temperature for  $AL > 1$ . To make the system quasi-2D a large value of anisotropy parameter along axial direction  $LAMBDA = 12.5$  is chosen so that the condition  $\mu \ll \hbar\omega_z$  is satisfied. With this condition the atoms are strongly confined along axial ( $z$ ) direction and they are frozen in the ground state. The size of the harmonic oscillator basis  $\varphi_i$  chosen to expand  $us$  and  $vs$  is determined by  $NBX=NBY=55$ . This optimal basis size is chosen to produce very low ( $\sim O(10^{-13})$ ) residuals while diagonalising the BdG matrix using ARPACK. Initially, the total the number of atoms in each species are chosen to be 2000 each ( $TN01 = TN02 = 2000$ ). The under relaxation parameter SUNDER is kept fixed at 0.1, and number of NG modes to skip is set to 4 ( $SKIP = 4$ ), this avoids divergence associated with the NG modes. The parameter ITMAX is the maximum

number of iterations to check the self consistency through HFB-Popov iterations of the BdG equations.

In addition to the parameters entered from the `input.dat`, there are other parameters and variables which are defined through modules in the main subroutine `hfb_main.f90`. The modules `COMM_DATA`, `GPE_DATA`, and `CN_DATA` are from the original GPE solver code [41–44]. Solving the HFB-Popov equations requires additional data and variables. For this we introduce two modules `HFB_2D_DATA` and `ARPK_DATA`. The former consists of arrays and constants pertaining to the BdG matrix and HFB-Popov approximation. These include arrays to store harmonic oscillator states  $\varphi$ , kinetic energy and potential energy contribution to BdG matrix, etc. The latter module has arrays and constants pertaining to `ARPACK`.

#### 4.2. Input data

Following input files are considered to show a testrun which takes  $\approx 10$  min to complete.

```

280.0D0    100.0D0    100.0D0    100.0D0    !Scattering lengths  G011,G012,G021,G022
133.0D0          87.0D0          !Masses              M1, M2
8.0D0          !Freq. along X drn.  NUR
1.0D0          12.5D0          !Anisotropy          AL, LAMBDA
200.0D0        200.0D0        !Number of atoms     TN01, TN02
0.1D0          !Underrelaxation     SUNDER
20             20             !Basis along X, Y    NBX, NBY
200            250            !NEV NCV
0.0D-9         !Temperature          TEMPK
4              1              !SKIP, ITMAX

```

#### 4.3. Output data

On successful completion of computation, the package generates the eigenvalues and eigen vectors of the BdG matrix. The eigenvalues are stored in data file `eigenvalue.out` and their corresponding quasiparticle amplitudes are stored in file `uv***.dat`. Where, `***` can take any value between 001 to 200. The details related to the computation are given in the output file `hfb2d2s.out`. Also, the eigen values and number of atoms at each HFB Popov iterations are written in `hfb2d2s.out`. To check for convergence in HFB-Popov iterations, one needs to follow the contents of output file `converge.out`. The contents of the `hfb2d2s.out` file for  $^{133}\text{Cs}$ - $^{87}\text{Rb}$  at temperature `0nk` are written below where `Norm1` and `Norm2` check the normalization, `<x1>` and `<x2>` calculate the rms sizes or radii for species 1 and 2 respectively. `Psi1^2(0)` and `Psi2^2(0)` state the density at the center of the confining potential for species 1 and 2 respectively.

---

Trapping potential, mass and temperature of the quasi-2D TBEC

---

ALPHA = 1.000, LAMBDA = 12.500

NUR = 8.000  
 M1 = 133.000, M2 = 87.000  
 G011 = 280.000, G012 = 100.000  
 G021 = 100.000, G022 = 100.000  
 BETA = Infinity

---

Derived constants, basis size and spatio-temporal grid information

---

Oscillator Length = 0.308263D-05  
 MRATIO(MASS1/MASS2) = 1.529  
 No. of basis X = 20  
 No. of basis Y = 20  
 No of spatial points NX = 200  
 No of spatial points NY = 200  
 Spatial step size DX = 0.050000  
 Spatial step size DY = 0.050000  
 Temporal step size DT = 0.001000

Total number of atoms  
 TN01 = 200.00, TN02 = 200.00

Number of iterations  
 NPAS = 5000 NRUN = 1000

---

iter	Norm1	Chem1	Ener	<x1>	Psi1 <sup>2</sup> (0)	N1T
	Norm2	Chem2		<x2>	Psi2 <sup>2</sup> (0)	N2T

---

Initial :

1.6686	1.0073	2.15965	0.94140	0.35917		
1.6686	1.1524		0.94140	0.35917		

After NPAS iterations:

0.9941	2.9792	3.33170	1.45698	0.11648		
0.9957	2.1750		1.60807	0.10136		

HFB-Popov iteration starts:

Temp=	0.0000000000000000E+000					
1	0.9941	2.9792	3.33170	1.45698	0.11648	0.00000
	0.9957	2.1750		1.60807	0.10136	0.00000

---

Eigen values correspondng to the Goldstone modes

---

nth state real(E\_n) img(E\_n)

---

1	-0.000000	0.000000
2	-0.000000	0.000000
3	-0.000000	0.000000
4	-0.000000	0.000000

---

Eigen values corresponding to quasi particle excitations

---

nth state	real(E_n)	img(E_n)
6	0.057608	0.000000
8	0.057610	0.000000
9	0.104018	0.000000
12	0.104018	0.000627
13	0.134642	-0.000627
15	0.134642	0.000000
18	0.253197	0.000000
19	0.696740	0.000000
20	0.696740	0.000000
23	0.862680	0.000000
25	0.863303	0.000000
27	0.868952	0.000000
29	0.869428	0.000000
31	0.892798	0.000000
32	0.892798	0.000000
35	0.893639	0.000000
37	0.893639	0.000000
39	0.894346	0.000000
41	1.000080	0.000000
44	1.000080	0.000000
46	1.051421	0.000000
48	1.051421	0.000000
49	1.099959	0.000000
51	1.099959	0.000000
**	*****	*****

---

Scaled coupling constants and condensate atoms at each iteration

---

Iter	G11	G12	G21	G22	N01	N02
Initial :						
	0.085195	0.038471	0.038471	0.046514	200.000000	200.000
1	16.991558	7.682903	7.672707	9.289328	199.443593	199.708
It took:	4.69246413310369		minutes.			

In the printout of the output file `hfb2d2s.out`, the rows with `*****` indicate the additional lines (corresponding to higher excited states) of data. For compactness of the manuscript, we have excluded the additional data of the same type. For shorter execution time of the test run with the above provided sample input file we have considered only one HFB-Popov iteration. In the eigen value spectrum, the eigenvalues corresponding to state 12 and 13 possess imaginary part as well. These imaginary parts have nothing to do with the instability of the system. Rather it is due to choice of basis size 20 which is insufficient for calculation but necessary for shorter execution time in `testrun`. `N01` and `N02` correspond to the number of condensate atoms for species 1 and 2 respectively. Though the eigenvalues are printed in `hfb2d2s.out`, for other detailed computations like the mode evolution as a function of anisotropy and interaction parameters, the energy eigenvalues are also stored in the output file `eigenvalue.out`. Such data is useful in studies like our previous works [16, 17], where we have shown the mode evolution as a function of various parameters using this package. It is to be mentioned that, the energy eigen values, chemical potentials and total energy of the system, calculated in this package are in units of  $\hbar\omega_x$ .

## 5. Numerical results

In this section, we describe the results from our code in different parameter regimes at zero temperature as well as in finite temperature. At zero temperature, the self-consistent HFB-Popov iterations do not produce significant changes in density profiles. Since, HFB Popov iterations are computationally expensive and take time, the results of zero temperature calculations are provided after single HFB-Popov iteration (`ITMAX` = 1). Whereas for finite temperature we consider `ITMAX` = 15 which provides required convergence.

In TBEC, the unique and easily observable effect is phase separation, where the density peaks of the component BECs are separate. Alternatively, we can say the miscible TBEC phase separates, and enters into immiscible configurations. Numerically, this is quantifiable from the overlap integral  $\Lambda$  as well as the quasi particle amplitudes. In two dimensional (as well as in quasi 2D) systems, the phase separation of TBEC can occur in two ways. First, the density peaks of the BECs get shifted either along  $x$ -axis or along  $y$ -axis in  $x$ - $y$  plane. This type of phase separation is referred to as *side-by-side* phase separation. And second possibility arises when one species occupies the core region while the second species surrounds the first one like an annular ring. This type of phase separated density profile is termed as *shell structured* density profile. In earlier kind of phase separation, the symmetry of the confining potential is broken where as it is preserved in the latter case.

### 5.1. Zero temperature

In this section we describe the zero temperature condensate density profiles  $n_{ic}$  and the Bogoliubov quasi particle amplitudes  $u$  and  $v$  in miscible and immiscible regions. In Fig. 1, we show the density of condensate atoms  $n_{ic}(x, 0)$ . This figure is obtained by plotting column 1, 3 and 5 of file `den00x.dat` for three different inter species

interaction strengths. If otherwise mentioned, in all the figures the species 1 and 2 correspond to  $^{133}\text{Cs}$  and  $^{87}\text{Rb}$ , respectively. For Fig.1(a) and Fig.1(c) we consider total 2000 of atoms where as in Fig.1(b) we consider total 5000 atoms. To obtain equilibrium ground states and avoid metastable states for side by side phase separated TBEC, it is essential to start the iterations with the initial guess wave functions having spatially separated peaks. This is implemented in the subroutine `initialize.f90` by setting `SHIFT1 = 5.0D0`. This also ensures rapid convergence. For other density configurations, `SHIFT1 = 0.0D0` is considered and implies complete overlap of the initial guess wave functions.

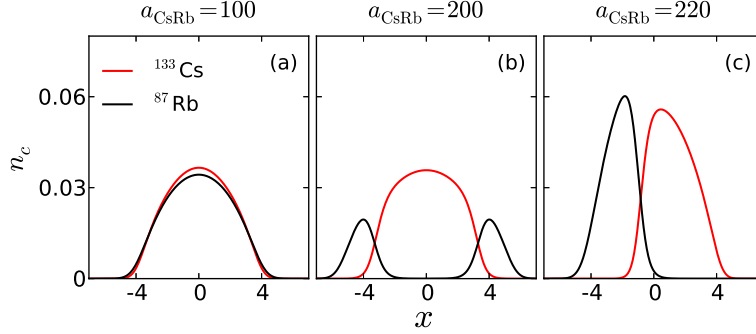


Figure 1: Equilibrium ground state of  $^{133}\text{Cs}$ - $^{87}\text{Rb}$  TBEC at zero temperature for three different values of interspecies interaction strength (a)  $a_{\text{CsRb}} = 100a_0$ : TBEC is in miscible domain (b)  $a_{\text{CsRb}} = 200a_0$ : TBEC is in shell-structured domain and (c)  $a_{\text{CsRb}} = 220a_0$ : TBEC is side-by-side phase separated.  $n_c$  is measured in units of  $a_{\text{osc}}^{-2}$  and the spatial coordinate  $x$  is measured in units of  $a_{\text{osc}}$ .

From Fig.1(b) it is clear that the TBEC shell-structured for the chosen set of parameters, where  $^{133}\text{Cs}$  BEC is at the core and with the  $^{87}\text{Rb}$  BEC surrounding it. In Fig.1(c),  $^{133}\text{Cs}$  and  $^{87}\text{Rb}$  BECs occupy right and left sides, respectively. Here, the positions of the BECs are not unique, and can interchange depending on the shift in initial guess wave functions. Below we provide content of the input file to corresponding to Fig.1(a).

*input file corresponding to Fig.1(a):*

```

280.0D0    100.0D0    100.0D0    100.0D0    !Scattering lengths G011,G012,G021,G022
133.0D0          87.0D0          !Masses M1, M2
8.0D0          !Freq. along X drn. NUR
1.0D0          12.5D0          !Anisotropy AL, LAMBDA
2000.0D0      2000.0D0      !Number of atoms TN01, TN02
0.1D0          !Underrelaxation SUNDER
55    55          !Basis along X, Y NBX, NBY
200    250          !NEV NCV
0.0D-9          !Temperature TEMPK
4    1          !SKIP, ITMAX

```

The formation of BEC is associated with the spontaneous symmetry breaking (SSB) of  $U(1)$  global gauge. Due to this SSB, in trapped quasi-2D TBEC, the low-energy

BdG spectrum has two Goldstone modes for each of the condensate species. In other words, the excitation spectrum of the BEC is gapless, and the two lowest energy modes with finite energies are the dipole modes. The dipole modes which oscillate out-of-phase with each other are called slosh modes. The in-phase slosh modes with center-of-mass motion are called the Kohn modes and have frequency identical to the natural frequency of the harmonic confining potential. Thus the frequency of the Kohn mode is independent of the type of interactions and interaction strength as well. For this reason, getting Kohn mode energy close to 1 serves as an important consistency check of our FACT package.

The Bogoliubov quasi particle amplitudes corresponding to low energy modes are shown in Fig. 2, 3 and 4 for miscible, side-by-side and shell-structured TBEC respectively.

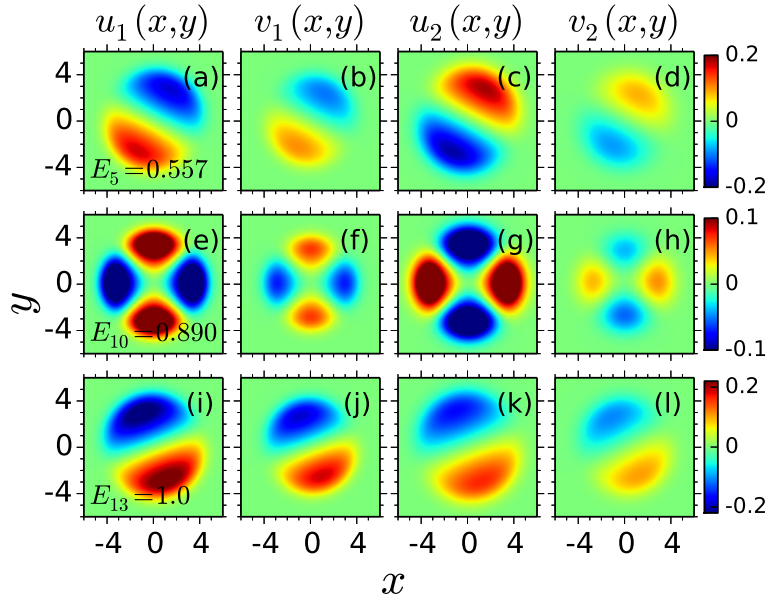


Figure 2: Quasiparticle amplitudes corresponding to miscible  $^{133}\text{Cs}$ - $^{87}\text{Rb}$  TBEC at zero temperature. (a)-(b) show slosh modes for species 1 and (c) - (d) corresponds to those of species 2. (e)-(f) show quadrupole modes for species 1 and (g) - (h) are those for species 2. (i)-(j) describe the Kohn mode corresponding to species 1 and (k) - (l) are those due to species 2.  $u$ s and  $v$ s are in units of  $a_{\text{osc}}^{-1}$  and spatial coordinate  $x$  and  $y$  are in units of  $a_{\text{osc}}$ .

The quasiparticle amplitudes of the selected low-energy modes in the miscible domain obtained with  $a_{\text{CsRb}} = 100a_0$  are shown in Fig. 2. The images in Fig. 2 (a)-(d) correspond to the slosh mode of the system. To obtain the quasiparticle amplitudes, we plot column 3, 4, 5 and 6 of file `uv005.dat`. In Fig. 2(e)-(h), the quasiparticle amplitudes from the file `uv010.dat` are shown, and these correspond to quadrupole mode of the system. And, the Kohn modes, from the data in the file `uv013.dat`, are shown in Fig. 2(i)-(l). Here, the numerical value 013 in file name `uv013.dat` indicates that it is the 13th excited state. For each of the quasiparticle amplitudes the

corresponding energies, taken from the output file `eigenvalue.dat`, are given in the bottom left corner.

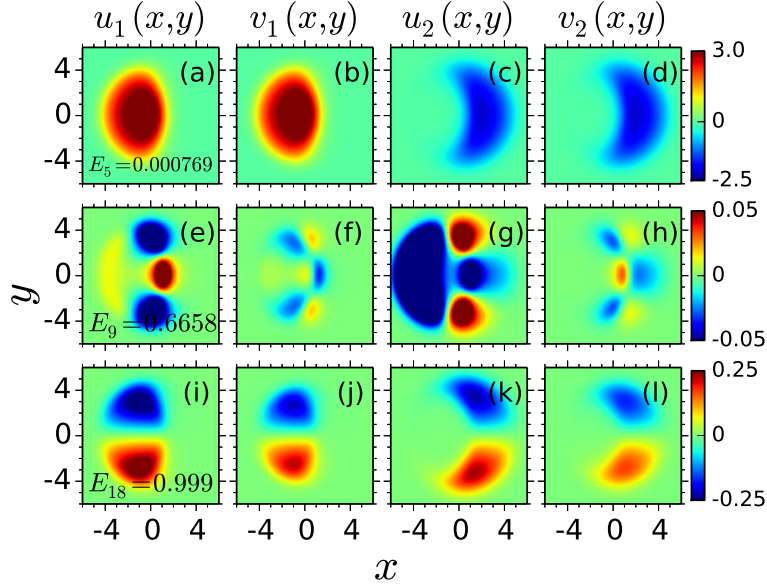


Figure 3: Quasiparticle amplitudes corresponding to side-by-side phase separated  $^{133}\text{Cs}$ - $^{87}\text{Rb}$  TBEC at zero temperature. (a)-(d) show quasiparticle amplitudes corresponding to NG mode for each of the species. (e)-(h) show those for interface mode for each species. (i)-(l) describe those corresponding to the Kohn mode for each of the species. Subscript indices 1 and 2 refer to species 1 and 2 respectively.  $u_s$  and  $v_s$  are in units of  $a_{\text{osc}}^{-1}$  and spatial coordinates  $x$  and  $y$  are in units of  $a_{\text{osc}}$ .

For the case of side-by-side immiscible phase, with  $a_{\text{CsRb}} = 220a_0$ , the quasiparticle amplitudes of low-lying modes are shown in Fig. 3. The images in Fig. 3 (a)-(d) correspond to the NG modes of the system which in general resemble  $n_{ic}$ , and are based on the data in the output file `uv005.dat`. Due to the rotational symmetry breaking associated with the miscible to side-by-side immiscible phase transition, each species has two additional NG modes. The Fig.3(e)-(h) show the quasiparticle amplitudes from `uv009.dat`, and these correspond to interface mode of the system. In the immiscible domain the interface modes, as the name suggests, are localized at the interface of the two species. The Kohn modes of the system are shown in Fig. 3(i)-(l) which correspond to the data in `uv018.dat`.

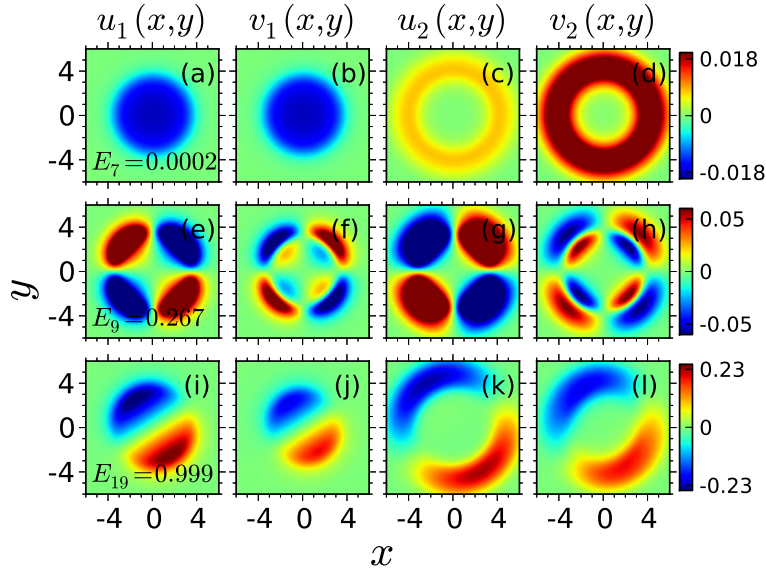


Figure 4: Quasiparticle amplitudes corresponding to shell structured  $^{133}\text{Cs}$ - $^{87}\text{Rb}$  TBEC at zero temperature. (a)-(d) show quasiparticle amplitudes corresponding to NG mode for each of the species. (e)-(h) show those for interface mode for each species. (i)-(l) describe those corresponding to the Kohn mode for each of the species. Like Fig.2 and Fig.3, subscript indices 1 and 2 refer to species 1 and 2 respectively.  $u_s$  and  $v_s$  are in units of  $a_{\text{osc}}^{-1}$  and spatial coordinates  $x$  and  $y$  are in units of  $a_{\text{osc}}$ .

For shell-structured TBEC, the quasiparticle amplitudes corresponding to NG modes, quadrupole modes and Kohn modes are shown in Fig.4(a)-(d), (e)-(h) and (i)-(l) respectively.

### 5.2. Finite temperature

For finite temperature computations, solving the HFB-Popov equations require iterations and we consider  $\text{ITMAX} = 15$  for all the finite temperature computations reported in this work. The density profiles of  $n_{ic}$  corresponding to each HFB-Popov iterations are stored in the file `den00x.dat` where  $x$  runs from 0 to ITMAX. When  $T \neq 0$ , at each iteration, the number of condensate atoms decreases, whereas the number of thermal (non condensate) atoms increases. Fig. 5 shows the equilibrium profiles of  $n_{ic}$  and  $\tilde{n}_{ic}$  for three different temperatures in miscible domain. The plots in Fig. 5(a) correspond to  $n_{ic}$  at  $T = 0\text{nK}$ , and hence in Fig. 5(d)  $\tilde{n}_{ic}$  are negligibly small. The plots in Fig. 5(b) and (c) correspond to  $n_{ic}$  at  $T = 5\text{nK}$  and  $T = 10\text{nK}$ , respectively. To obtain the plots in the top row, we plotted column 1, column 3 and column 5 file of `den00x.dat` with column 3 and column 5 multiplied by number of condensate atoms  $N_{01}$  and  $N_{02}$  (taken from `hfb2d2s.out`), respectively. Although, the changes in  $n_{ic}$  are not dramatic, there is a large change in  $\tilde{n}_{ic}$  as shown in Fig.5(e)-(f). From Fig. 5, there is a notable feature of  $\tilde{n}_{ic}$ : it has a minimum where  $n_{ic}$  has maximum value.

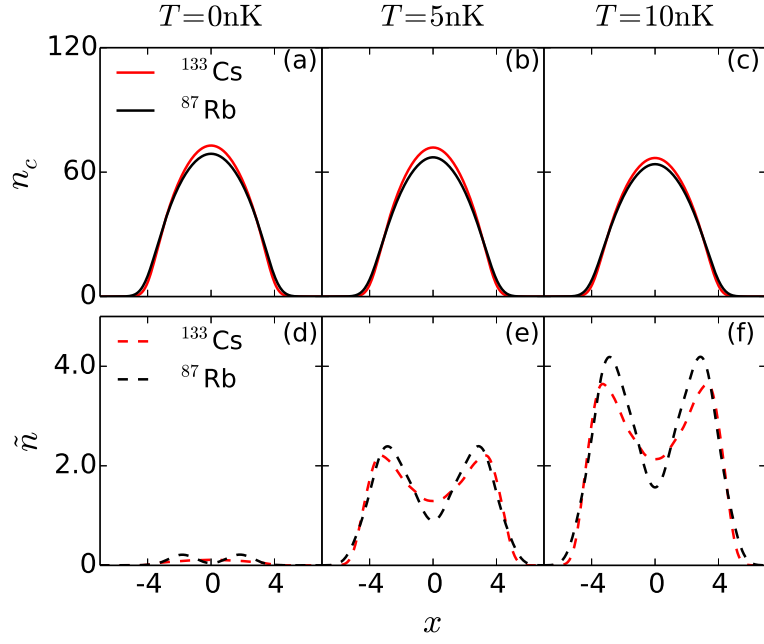


Figure 5: Equilibrium ground state density of  $^{133}\text{Cs}$ - $^{87}\text{Rb}$  TBEC in miscible domain for three different values of temperature (a)  $T = 0\text{nK}$  (b)  $T = 5\text{nK}$  and (c)  $T = 10\text{nK}$ . Interspecies interaction strength is fixed at  $a_{\text{CsRb}} = 100a_0$ .  $n_c$  and  $\tilde{n}$  are measured in units of  $a_{\text{osc}}^{-2}$  and the spatial coordinate  $x$  is measured in units of  $a_{\text{osc}}$ .

For the side-by-side configuration the density profiles at finite temperature are shown in Fig. 6. Like in the miscible domain, here as well, we observe growth in  $\tilde{n}_{ic}$  with the increase of temperature and thereby lowering the number of condensate atoms. It is to be noted that at the interface of two species, where the  $n_{ic}$  are low,  $\tilde{n}_{ic}$  have maximum value.

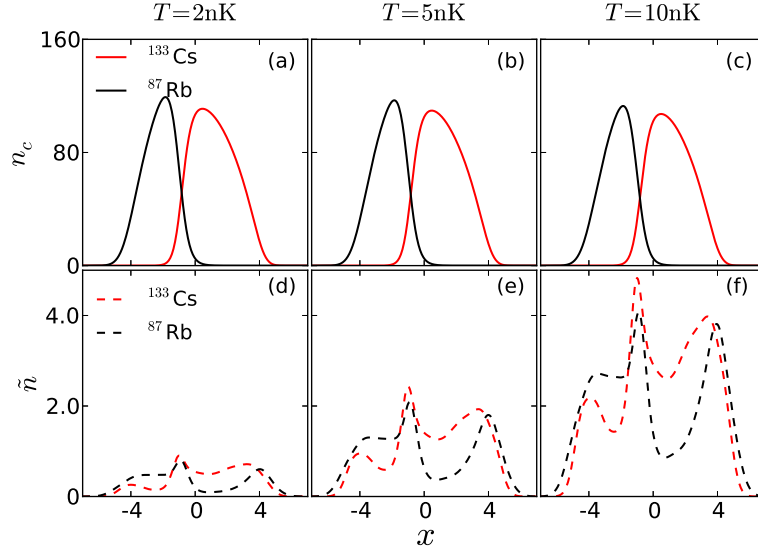


Figure 6: Equilibrium ground state density of  $^{133}\text{Cs}$ - $^{87}\text{Rb}$  TBEC in immiscible (side-by-side) domain for three different values of temperature (a)  $T = 2\text{nK}$  (b)  $T = 5\text{nK}$  and (c)  $T = 10\text{nK}$ . Interspecies interaction strength is fixed at  $a_{\text{CsRb}} = 220a_0$ .  $n_c$  and  $\tilde{n}$  are measured in units of  $a_{\text{osc}}^{-2}$  and the spatial coordinate  $x$  is measured in units of  $a_{\text{osc}}$ .

## Acknowledgments

The example results shown in the paper are based on the computations using the HPC cluster Vikram-100 at Physical Research Laboratory, Ahmedabad and Max Planck Computing Facility. S. G. acknowledges the support of the Science & Engineering Research Board (SERB), Department of Science and Technology, Government of India under the project ECR/2017/001436 and ISIRD project 9-256/2016/IITRPR/823 of Indian Institute of Technology (IIT) Ropar.

## References

- [1] A. Griffin, *Phys. Rev. B* **53**, 9341 (1996).
- [2] D. A. W. Hutchinson, E. Zaremba, and A. Griffin, *Phys. Rev. Lett.* **78**, 1842 (1997).
- [3] R. J. Dodd, M. Edwards, C. W. Clark, and K. Burnett, *Phys. Rev. A* **57**, R32 (1998).
- [4] C. Gies, B. P. van Zyl, S. A. Morgan, and D. A. W. Hutchinson, *Phys. Rev. A* **69**, 023616 (2004).
- [5] D. S. Jin, M. R. Matthews, J. R. Ensher, C. E. Wieman, and E. A. Cornell, *Phys. Rev. Lett.* **78**, 764 (1997).

- [6] S. Gautam and D. Angom, *Journal of Physics B: Atomic, Molecular and Optical Physics* **44**, 025302 (2011).
- [7] S. Gautam and D. Angom, *Phys. Rev. A* **81**, 053616 (2010).
- [8] M. O. C. Pires and E. J. V. de Passos, *Phys. Rev. A* **77**, 033606 (2008).
- [9] A. Roy, S. Gautam, and D. Angom, *Phys. Rev. A* **89**, 013617 (2014).
- [10] A. Roy and D. Angom, *Phys. Rev. A* **92**, 011601 (2015).
- [11] A. Roy and D. Angom, *New Journal of Physics* **18**, 083007 (2016).
- [12] C. R. Cabrera, L. Tanzi, J. Sanz, B. Naylor, P. Thomas, P. Cheiney, and L. Tarruell, *Science* **359**, 301 (2018).
- [13] D. S. Petrov, *Phys. Rev. Lett.* **115**, 155302 (2015).
- [14] D. S. Petrov and G. E. Astrakharchik, *Phys. Rev. Lett.* **117**, 100401 (2016).
- [15] G. Semeghini, G. Ferioli, L. Masi, C. Mazzinghi, L. Wolswijk, F. Minardi, M. Modugno, G. Modugno, M. Inguscio, and M. Fattori, *Phys. Rev. Lett.* **120**, 235301 (2018).
- [16] S. Pal, A. Roy, and D. Angom, *J. Phys. B.* **50**, 195301 (2017).
- [17] S. Pal, A. Roy, and D. Angom, *J. Phys. B* **51**, 085302 (2018).
- [18] P. Hohenberg and P. Martin, *Annals of Physics* **34**, 291 (1965).
- [19] N. D. Mermin and H. Wagner, *Phys. Rev. Lett.* **17**, 1133 (1966).
- [20] V. L. Berezinskii, *Sov. Phys. JETP* **34**, 610 (1972).
- [21] J. M. Kosterlitz and D. J. Thouless, *Journal of Physics C: Solid State Physics* **5**, L124 (1972).
- [22] J. M. Kosterlitz and D. J. Thouless, *Journal of Physics C: Solid State Physics* **6**, 1181 (1973).
- [23] J. M. Kosterlitz, *Rep. Prog. Phys.* **79**, 026001 (2016).
- [24] J. L. Ville, R. Saint-Jalm, E. Le Cerf, M. Aidelsburger, S. Nascimbène, J. Dalibard, and J. Beugnon, *Phys. Rev. Lett.* **121**, 145301 (2018).
- [25] K. Suthar, A. Roy, and D. Angom, *Phys. Rev. A* **91**, 043615 (2015).
- [26] K. Suthar and D. Angom, *Phys. Rev. A* **93**, 063608 (2016).
- [27] Z. Bai and R.-C. Li, *Siam J. Matrix Anal. Appl.* **33**, 1075 (2012).
- [28] Z. Bai and R.-C. Li, *BIT Numerical Mathematics* **54**, 31 (2014).

- [29] D. S. Petrov, M. Holzmann, and G. V. Shlyapnikov, *Phys. Rev. Lett.* **84**, 2551 (2000).
- [30] L. Salasnich, A. Parola, and L. Reatto, *Phys. Rev. A* **65**, 043614 (2002).
- [31] D. S. Petrov, G. V. Shlyapnikov, and J. T. M. Walraven, *Phys. Rev. Lett.* **85**, 3745 (2000).
- [32] R. Lehoucq, D. Sorensen, and C. Yang, *ARPACK Users' Guide* (Society for Industrial and Applied Mathematics (Philadelphia), 1998).
- [33] P. Jain and M. Boninsegni, *Phys. Rev. A* **83**, 023602 (2011).
- [34] C. Ticknor, *Phys. Rev. A* **89**, 053601 (2014).
- [35] R. M. Wilson, S. Ronen, and J. L. Bohn, *Phys. Rev. Lett.* **104**, 094501 (2010).
- [36] F. Zambelli, L. Pitaevskii, D. M. Stamper-Kurn, and S. Stringari, *Phys. Rev. A* **61**, 063608 (2000).
- [37] D. M. Stamper-Kurn, A. P. Chikkatur, A. Görlitz, S. Inouye, S. Gupta, D. E. Pritchard, and W. Ketterle, *Phys. Rev. Lett.* **83**, 2876 (1999).
- [38] J. Stenger, S. Inouye, A. P. Chikkatur, D. M. Stamper-Kurn, D. E. Pritchard, and W. Ketterle, *Phys. Rev. Lett.* **82**, 4569 (1999).
- [39] W.-C. Wu and A. Griffin, *Phys. Rev. A* **54**, 4204 (1996).
- [40] C. Menotti, M. Krämer, L. Pitaevskii, and S. Stringari, *Phys. Rev. A* **67**, 053609 (2003).
- [41] P. Muruganandam and S. Adhikari, *Comput. Phys. Commun.* **180**, 1888 (2009).
- [42] D. Vudragović, I. Vidanović, A. Balaž, P. Muruganandam, and S. K. Adhikari, *Comput. Phys. Commun.* **183**, 2021 (2012).
- [43] L. E. Young-S., D. Vudragović, P. Muruganandam, S. K. Adhikari, and A. Balaž, *Comput. Phys. Commun.* **204**, 209 (2016).
- [44] L. E. Young-S., P. Muruganandam, S. K. Adhikari, V. Lončar, D. Vudragović, and A. Balaž, *Comput. Phys. Commun.* **220**, 503 (2017).
- [45] A. Minguzzi, S. Succi, F. Toschi, M. Tosi, and P. Vignolo, *Physics Reports* **395**, 223 (2004).
- [46] X. Antoine, W. Bao, and C. Besse, *Computer Physics Communications* **184**, 2621 (2013).
- [47] W. Bao, *Multiscale Model. Simul.* **2**, 210 (2004).
- [48] W. Bao and J. Shen, *SIAM J. Sci. Comput.* **26**, 2010 (2005).
- [49] R. P. Tiwari and A. Shukla, *Computer Physics Communications* **174**, 966 (2006).
- [50] T. Simula, S. Virtanen, and M. Salomaa, *Comput. Phys. Commun.* **142**, 396 (2001).

## 6. Appendix

The explicit forms of  $\hat{H}_n^i$ , where  $0 \leq n \leq 4$  and  $i = 1, 2$  represent the order of fluctuations and species index, are

$$\begin{aligned}
\hat{H}_0^1 &= \iint dxdy \phi_1^* \left( \hat{h}_1 - \mu_1 + \frac{U_{11}}{2} |\phi_1|^2 + \frac{U_{12}}{2} |\phi_2|^2 \right) \phi_1, \\
\hat{H}_0^2 &= \iint dxdy \phi_2^* \left( \hat{h}_2 - \mu_2 + \frac{U_{22}}{2} |\phi_2|^2 + \frac{U_{12}}{2} |\phi_1|^2 \right) \phi_2, \\
\hat{H}_1^1 &= \iint dxdy \left[ \phi_1^* \left( \hat{h}_1 - \mu_1 + U_{11} |\phi_1|^2 + U_{12} |\phi_2|^2 \right) \tilde{\psi}_1 + \tilde{\psi}_1^\dagger \left( \hat{h}_1 - \mu_1 + U_{11} |\phi_1|^2 + U_{12} |\phi_2|^2 \right) \phi_1 \right], \\
\hat{H}_1^2 &= \iint dxdy \left[ \phi_2^* \left( \hat{h}_2 - \mu_2 + U_{22} |\phi_2|^2 + U_{12} |\phi_1|^2 \right) \tilde{\psi}_2 + \tilde{\psi}_2^\dagger \left( \hat{h}_2 - \mu_2 + U_{22} |\phi_2|^2 + U_{12} |\phi_1|^2 \right) \phi_2 \right], \\
\hat{H}_2^1 &= \iint dxdy \left[ \tilde{\psi}_1^\dagger \left( \hat{h}_1 - \mu_1 + 2U_{11} |\phi_1|^2 + U_{12} |\phi_2|^2 \right) \tilde{\psi}_1 + \frac{U_{11}}{2} \left( \phi_1^{*2} \tilde{\psi}_1 \tilde{\psi}_1 + \phi_1^2 \tilde{\psi}_1^\dagger \tilde{\psi}_1^\dagger \right) \right. \\
&\quad \left. + \frac{U_{12}}{2} \left( \phi_1^* \phi_2^* \tilde{\psi}_1 \tilde{\psi}_2 + \phi_1^* \phi_2 \tilde{\psi}_2^\dagger \tilde{\psi}_1 + \phi_1 \phi_2^* \tilde{\psi}_1^\dagger \tilde{\psi}_2 + \phi_1 \phi_2 \tilde{\psi}_1^\dagger \tilde{\psi}_2^\dagger \right) \right], \\
\hat{H}_2^2 &= \iint dxdy \left[ \tilde{\psi}_2^\dagger \left( \hat{h}_2 - \mu_2 + 2U_{22} |\phi_2|^2 + U_{12} |\phi_1|^2 \right) \tilde{\psi}_2 + \frac{U_{22}}{2} \left( \phi_2^{*2} \tilde{\psi}_2 \tilde{\psi}_2 + \phi_2^2 \tilde{\psi}_2^\dagger \tilde{\psi}_2^\dagger \right) \right. \\
&\quad \left. + \frac{U_{12}}{2} \left( \phi_1^* \phi_2^* \tilde{\psi}_1 \tilde{\psi}_2 + \phi_1^* \phi_2 \tilde{\psi}_2^\dagger \tilde{\psi}_1 + \phi_1 \phi_2^* \tilde{\psi}_1^\dagger \tilde{\psi}_2 + \phi_1 \phi_2 \tilde{\psi}_1^\dagger \tilde{\psi}_2^\dagger \right) \right], \\
\hat{H}_3^1 &= \iint dxdy \left[ U_{11} \left( \phi_1^* \tilde{\psi}_1^\dagger \tilde{\psi}_1 \tilde{\psi}_1 + \phi_1 \tilde{\psi}_1^\dagger \tilde{\psi}_1^\dagger \tilde{\psi}_1 \right) + \frac{U_{12}}{2} \left( \phi_1^* \tilde{\psi}_2^\dagger \tilde{\psi}_1 \tilde{\psi}_2 + \phi_2^* \tilde{\psi}_1^\dagger \tilde{\psi}_1 \tilde{\psi}_2 \right) \right. \\
&\quad \left. + \phi_1 \tilde{\psi}_1^\dagger \tilde{\psi}_2^\dagger \tilde{\psi}_2 + \phi_2 \tilde{\psi}_1^\dagger \tilde{\psi}_2^\dagger \tilde{\psi}_1 \right], \\
\hat{H}_3^2 &= \iint dxdy \left[ U_{22} \left( \phi_2^* \tilde{\psi}_2^\dagger \tilde{\psi}_2 \tilde{\psi}_2 + \phi_2 \tilde{\psi}_2^\dagger \tilde{\psi}_2^\dagger \tilde{\psi}_2 \right) + \frac{U_{12}}{2} \left( \phi_1^* \tilde{\psi}_2^\dagger \tilde{\psi}_1 \tilde{\psi}_2 + \phi_2^* \tilde{\psi}_1^\dagger \tilde{\psi}_1 \tilde{\psi}_2 \right) \right. \\
&\quad \left. + \phi_1 \tilde{\psi}_1^\dagger \tilde{\psi}_2^\dagger \tilde{\psi}_2 + \phi_2 \tilde{\psi}_1^\dagger \tilde{\psi}_2^\dagger \tilde{\psi}_1 \right], \\
\hat{H}_4^1 &= \iint dxdy \left[ \frac{U_{11}}{2} \tilde{\psi}_1^\dagger \tilde{\psi}_1^\dagger \tilde{\psi}_1 \tilde{\psi}_1 + \frac{U_{12}}{2} \tilde{\psi}_1^\dagger \tilde{\psi}_2^\dagger \tilde{\psi}_1 \tilde{\psi}_2 \right], \\
\hat{H}_4^2 &= \iint dxdy \left[ \frac{U_{22}}{2} \tilde{\psi}_2^\dagger \tilde{\psi}_2^\dagger \tilde{\psi}_2 \tilde{\psi}_2 + \frac{U_{12}}{2} \tilde{\psi}_1^\dagger \tilde{\psi}_2^\dagger \tilde{\psi}_1 \tilde{\psi}_2 \right]. \tag{37}
\end{aligned}$$

Using the definition of field operator from Eq. (5) and putting it in Eq. (4), the Heisenberg equation of motion for the first species ( $i = 1$ ) is

$$\begin{aligned}
i\hbar \frac{\partial(\phi_1 + \tilde{\psi}_1)}{\partial t} &= \left[ \frac{-\hbar^2}{2m_1} \nabla^2 \phi_1 - \frac{\hbar^2}{2m_1} \nabla^2 \tilde{\psi}_1 + V_1 \phi_1 + V_1 \tilde{\psi}_1 \right. \\
&\quad \left. + U_{11} \hat{\Psi}_1^\dagger \hat{\Psi}_1 \hat{\Psi}_1 + U_{12} \hat{\Psi}_2^\dagger \hat{\Psi}_2 \hat{\Psi}_1 - \mu_1 \phi_1 - \mu_1 \tilde{\psi}_1 \right]. \tag{38}
\end{aligned}$$

The interaction terms in the equation can be written in terms of  $c$ -number and fluctuation operators as

$$\hat{\Psi}_1^\dagger \hat{\Psi}_1 \hat{\Psi}_1 = |\phi_1|^2 \phi_1 + 2|\phi_1|^2 \tilde{\psi}_1 + 2\phi_1 \tilde{\psi}_1^\dagger \tilde{\psi}_1 + \phi_1^* \tilde{\psi}_1 \tilde{\psi}_1 + \phi_1^2 \tilde{\psi}_1^\dagger + \tilde{\psi}_1^\dagger \tilde{\psi}_1 \tilde{\psi}_1, \quad (39a)$$

$$\begin{aligned} \hat{\Psi}_2^\dagger \hat{\Psi}_2 \hat{\Psi}_1 &= |\phi_2|^2 \phi_1 + |\phi_2|^2 \tilde{\psi}_1 + \phi_2^* \tilde{\psi}_2 \phi_1 + \phi_2^* \tilde{\psi}_2 \tilde{\psi}_1 + \tilde{\psi}_2^\dagger \phi_2 \phi_1 + \tilde{\psi}_2^\dagger \phi_2 \tilde{\psi}_1 \\ &\quad + \tilde{\psi}_2^\dagger \tilde{\psi}_2 \phi_1 + \tilde{\psi}_2^\dagger \tilde{\psi}_2 \tilde{\psi}_1. \end{aligned} \quad (39b)$$

Since all the atomic fluctuations (quantum and thermal) associated in this theory are white noise  $\langle \tilde{\psi}_i \rangle = \langle \tilde{\psi}_i^\dagger \rangle = 0$ . Hence the expectation value of the product of operators are

$$\langle \hat{\Psi}_1^\dagger \hat{\Psi}_1 \hat{\Psi}_1 \rangle = |\phi_1|^2 \phi_1 + \phi_1^* \langle \tilde{\psi}_1 \tilde{\psi}_1 \rangle + 2\phi_1 \langle \tilde{\psi}_1^\dagger \tilde{\psi}_1 \rangle + \langle \tilde{\psi}_1^\dagger \tilde{\psi}_1 \tilde{\psi}_1 \rangle, \quad (40a)$$

$$\begin{aligned} \langle \hat{\Psi}_2^\dagger \hat{\Psi}_2 \hat{\Psi}_1 \rangle &= |\phi_1|^2 \phi_1 + \phi_2^* \langle \tilde{\psi}_2 \tilde{\psi}_1 \rangle + \phi_2 \langle \tilde{\psi}_2^\dagger \tilde{\psi}_1 \rangle + \phi_1 \langle \tilde{\psi}_2^\dagger \tilde{\psi}_2 \rangle \\ &\quad + \langle \tilde{\psi}_2^\dagger \tilde{\psi}_2 \tilde{\psi}_1 \rangle. \end{aligned} \quad (40b)$$

Considering that the fluctuations of the two species are uncorrelated  $\langle \tilde{\psi}_2 \tilde{\psi}_1 \rangle = \langle \tilde{\psi}_2^\dagger \tilde{\psi}_1 \rangle = 0$ , the equation of motion of the condensate of the first species is obtained by taking the average of Eq. (38) as

$$\begin{aligned} i\hbar \frac{\partial \phi_1}{\partial t} &= \left[ -\frac{\hbar^2}{2m_1} \nabla^2 + V_1 - \mu_1 \right] \phi_1 + U_{11} [n_{1c} + 2\tilde{n}_1] \phi_1 + U_{11} \tilde{m}_1 \phi_1^* \\ &\quad + U_{12} [n_{2c} + \tilde{n}_2] \phi_1 + \langle \tilde{\psi}_1^\dagger \tilde{\psi}_1 \tilde{\psi}_1 \rangle + \langle \tilde{\psi}_2^\dagger \tilde{\psi}_2 \tilde{\psi}_1 \rangle. \end{aligned} \quad (41)$$

Similarly, the equation of motion for the condensate of the second species is

$$\begin{aligned} i\hbar \frac{\partial \phi_2}{\partial t} &= \left[ -\frac{\hbar^2}{2m_2} \nabla^2 + V_2 - \mu_2 \right] \phi_2 + U_{22} [n_{2c} + 2\tilde{n}_2] \phi_2 + U_{22} \tilde{m}_2 \phi_2^* \\ &\quad + U_{12} [n_{1c} + \tilde{n}_1] \phi_2 + \langle \tilde{\psi}_2^\dagger \tilde{\psi}_2 \tilde{\psi}_2 \rangle + \langle \tilde{\psi}_1^\dagger \tilde{\psi}_1 \tilde{\psi}_2 \rangle, \end{aligned} \quad (42)$$

where we have introduced the local densities:  $n_{ic} \equiv |\phi_i|^2$ ,  $\tilde{n}_i \equiv \langle \tilde{\psi}_i^\dagger \tilde{\psi}_i \rangle$ ,  $\tilde{m}_i \equiv \langle \tilde{\psi}_i \tilde{\psi}_i \rangle$  as the condensate, non-condensate, and anomalous densities, respectively. The equation of motion for the non-condensate density of the first species is

$$i\hbar \frac{\partial \tilde{\psi}_1}{\partial t} = i\hbar \frac{\partial}{\partial t} (\hat{\psi}_1 - \phi_1). \quad (43)$$

Using Eq. (38) and Eq. (41) and applying mean-field approximation,  $\tilde{\psi}_i^\dagger \tilde{\psi}_j \simeq \langle \tilde{\psi}_i^\dagger \tilde{\psi}_j \rangle$ ,  $\tilde{\psi}_i \tilde{\psi}_j \simeq \langle \tilde{\psi}_i \tilde{\psi}_j \rangle$ ,  $\tilde{\psi}_1^\dagger \tilde{\psi}_1 \tilde{\psi}_1 \simeq 2\langle \tilde{\psi}_1^\dagger \tilde{\psi}_1 \rangle \tilde{\psi}_1 + \langle \tilde{\psi}_1 \tilde{\psi}_1 \rangle \tilde{\psi}_1^\dagger$ ,  $\tilde{\psi}_2^\dagger \tilde{\psi}_2 \tilde{\psi}_1 \simeq \langle \tilde{\psi}_2^\dagger \tilde{\psi}_2 \rangle \tilde{\psi}_1$ , we can derive the equation of motion of the fluctuation operators.